ADVANCED OPTICAL MATERIALS
www.advopticalmat.de

Bidispersed Colloidal Assemblies Containing Xanthommatin Produce Angle-Independent Photonic Structures

*Zhuangsheng Lin, Zhe Gong, Duncan Q. Bower, Daeyeon Lee, and Leila F. Deravi**

The biological chromophore xanthommatin (Xa) contributes to the yellow, red, and brown colors and hues in cephalopods and arthropods. In many cases, Xa is also present as part of or coupled to supramolecular nanostructures, whose function has yet to be fully explored. To investigate how such structural elements impact the perceived color of these natural chromophores, amorphous photonic assemblies containing Xa chemically coupled to 100 nm polystyrene nanoparticles (PS100-XA) are fabricated, and blended with pure polystyrene (PS) nanoparticles of varying sizes. Structural colors are observed comprising these bidispersed colloidal assemblies that are tuned by the particle size of PS nanoparticles, the concentration of PS100-XA, the local environment, and the method of assembly. In all cases, the addition of PS100-XA regulates the color hue and contrast of the resultant assemblies by increasing light absorption while minimizing incoherent light scattering. Taken together, the results demonstrate how biochromes like Xa can enhance the color intensity and the diversity in colors present in common photonic assemblies.

1. Introduction

Combinations of absorptive pigments and arrayed light-scattering, interfering, or diffracting nanostructures are known to contribute to dynamic colors in nature.[1] For example, the feather barbules of the bird of paradise *Parotia lawesii* consist of layers of fibrous and noncrystalline keratin proteins (diameter ≈ 400 nm) and melanin-containing particles (diameter ≈ 250 nm) that are present in alternating layers to produce thin-film interference and iridescent colors that range from blue to yellow.[2] On the other hand, pierid butterflies incorporate yellow pterin pigments that are deposited within oblong granules (length ≈ 400 nm, width ≈ 150 nm) adjacent to chitin nanostructures in their wing scales.[3] This combination contributes to both broadband scattering and wavelength specific light absorption.[3,4] Our group has also recently reported the interplay of xanthommatin (Xa)-based pigment granules and protein-based structural elements in the dermal chromatophore organs of squid *Doryteuthis pealeii* that produce a patchy iridescence of blue, green, yellow, and red colors within the same chromatocyte.[5] These observations point to a synergistic relationship between biochromes like Xa and supramolecular nanostructures that have yet to be explored in regulating tunable structural colors.

In synthetic systems, the addition of biological pigments with or within artificial photonic assemblies has already shown exciting potential in regulating color hue and color purity of materials, warranting their further exploration for consumer applications such as coatings, cosmetics, apparel, and display design.[6–9] One example is the application of high refractive index melanin-based pigments incorporated into photonic assemblies to improve the color purity of a heterogeneous population of nanostructures. For example, Zhang et al. demonstrated this concept by mixing melanin-containing cuttlefish ink particles (diameter of 110 nm) with spherical polystyrene nanoparticles (diameters of 200–280 nm) to produce noniridescent amorphous photonic crystals.[6] Xiao et al. separately synthesized photonic films using melanin-inspired nanoparticles (diameter ≈ 100 nm) to produce a diverse array of colors that were governed by the thickness of the coatings.[7] Inspired by all of the advancements made using these melanin-based[6–10] and even non-melanin (e.g., pterin)[3] photonic structures, we asked whether other nonblack pigments that have a similarly high refractive index, such as Xa (yellow/red), can be used to design artificial photonic materials with tunable coloration.

As a natural biochrome, Xa is found in pigment granules located within dermal chromatophore organs of cephalopods[5,11] and in the eyes, skin, and eggs of arthropods (e.g., dragonflies, butterflies, silkworms, and spiders).[12] Xa has a high reported refractive index range with a broad absorption profile.[13] Specifically, the real-portion of the RI for squid-extracted xanthommatin was reported to be 1.92, 1.95, 1.88, and 1.73 in acidified-methanol, methanol, 50/50 methanol/water, and 0.2 M NaOH, respectively.[13] To evaluate how the absorptive profile of these yellow/red pigments change when incorporated into nanostructures, we prepared bidispersed colloidal assemblies using Xa tethered to 100 nm polystyrene (PS) spheres (PS100-XA) that were blended into variable suspensions of monodispersed PS nanoparticles (200–300 nm in diameter).

Z. Lin, D. Q. Bower, L. F. Deravi
Department of Chemistry and Chemical Biology
Northeastern University
102 HT (Hurtig Hall), Boston, MA 02115, USA
E-mail: l.deravi@northeastern.edu
Z. Gong, D. Lee
Department of Chemical and Biomolecular Engineering
University of Pennsylvania
Philadelphia, PA 19104, USA
The ORCID identification number(s) for the author(s) of this article can be found under https://doi.org/10.1002/adom.202100416.

DOI: 10.1002/adom.202100416

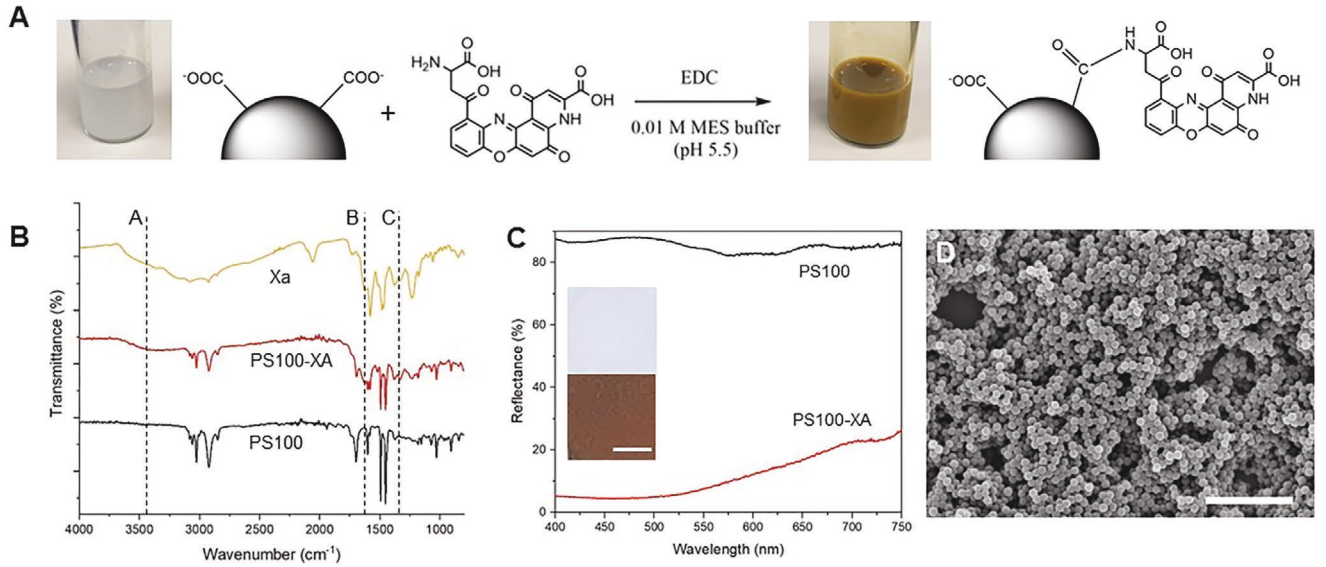

Figure 1. Xanthommatin functionalized nanoparticle synthesis on 100 nm polystyrene beads (PS100-XA): A) The synthesis scheme including xanthommatin in its nonionized form; B) ATR-FTIR spectra of pure Xa, PS100, and PS100-XA; C) reflectance spectra of PS100-XA (insert: photographic images of drop-casted PS100 (top) and PS100-XA (bottom) films; scale bar = 1 cm); D) representative SEM micrograph of PS100-XA (scale bar = 1 µm).

The optical properties of the resulting amorphous photonic assemblies were characterized as a function of packing density and environment, as we investigated their utility for tunable noniridescent structural colorants.

2. Results and Discussion

Upon coupling Xa, the concentrated suspension of PS nanoparticles (PS100-XA) displayed a brown color, which differed significantly from the bright white unfunctionalized control (PS100, **Figure 1**A). Pigment incorporation was also supported with ATR-FTIR spectra (Figure 1B), which showed a broad transmittance band at 3400 cm^{-1} (Figure 1B, band A) indicative of N–H stretching from amide groups between Xa and the carboxylic acid functionalized particles as seen in previous reports.[14,15] The transmittance bands around 1320 and 1650 cm^{-1} further supported the presence amide bonds, suggesting that Xa had successfully coupled onto the PS100 nanoparticles. This finding was also reinforced by the reduction of available carboxylic acid groups on the PS100 nanoparticles calculated from before and after EDC coupling using zeta potential measurements (Table S1, Supporting Information). This extrapolated density change in surface-accessible carboxylic acid groups was also utilized to approximate the Xa loading density on the nanoparticles,[16] which was estimated to be 4.0 ± 0.4 nmol μg^{-1} nanoparticles (N = 3). Based on these values, we calculated that ≈63 wt% of Xa had successfully coupled onto each particle.

Next, the visible color of the particles drop-casted as thin films was analyzed (Figure 1C). Not surprisingly, the control PS100 films displayed a white color, reflecting ≈85% of visible light; whereas, the PS100-XA film displayed a brown color with a relatively low reflectance (≈10%) at 400–500 nm region with an inflection of 23% from 600–700 nm. The reflectance profile of the PS100-XA was attributed to the absorption feature of Xa pigment, which has a characteristic absorption maximum of 430 nm in its oxidized form.[15,17] The particle size of the PS100-XA nanostructures was determined to 93 ± 5 nm using SEM analysis (Figure 1D, N = 20 particles), indicating that functionalization did not significantly alter the template size (reported as 100 nm).

We asked whether these pigmented particles could be used to create photonic assemblies with tunable visible colors and enhanced color contrast. To test this, we first created a bidispersed colloidal assembly containing mixtures of PS100-XA and pure PS nanoparticles of variable sizes, then used rapid centrifugation to sediment all particles to the bottom of the centrifuge tube (illustrated in **Figure 2**A). The subsequent materials demonstrated notable structural colors, where the observed hue was modulated by the particle size of the pure, un-functionalized PS nanoparticles (Figure 2B). The photonic assemblies retained the structural color when ground into powder (Figure 2C), suggesting the structures remained intact at the nanoscale. The mixed nanoparticles formed an amorphous array without any long-range order and periodicity (Figure 2D; Figure S1, Supporting Information), which was consistent with photonic glass shown in other studies.[6,18] Blending two particles of different sizes, in fact, is a well-established method of producing glassy assemblies.[8,19,20] These structures differed from the 3D photonic crystals (Figure S2, Supporting Information) formed by the pure monodispersed PS particles.

Given that the presence of PS100-XA nanoparticles altered the packing of pure PS particles, leading to amorphous photonic assemblies, we asked how the size ratio of the two particles as well as the concentration of the larger PS particles impacted the reflected colors. To test this, we first synthesized and processed pellets containing the photonic material comprising variations in PS particle sizes and concentrations of PS100-XA (**Figure 3**A). We observed that the resultant hue was controlled by the size of the PS nanoparticles, while the

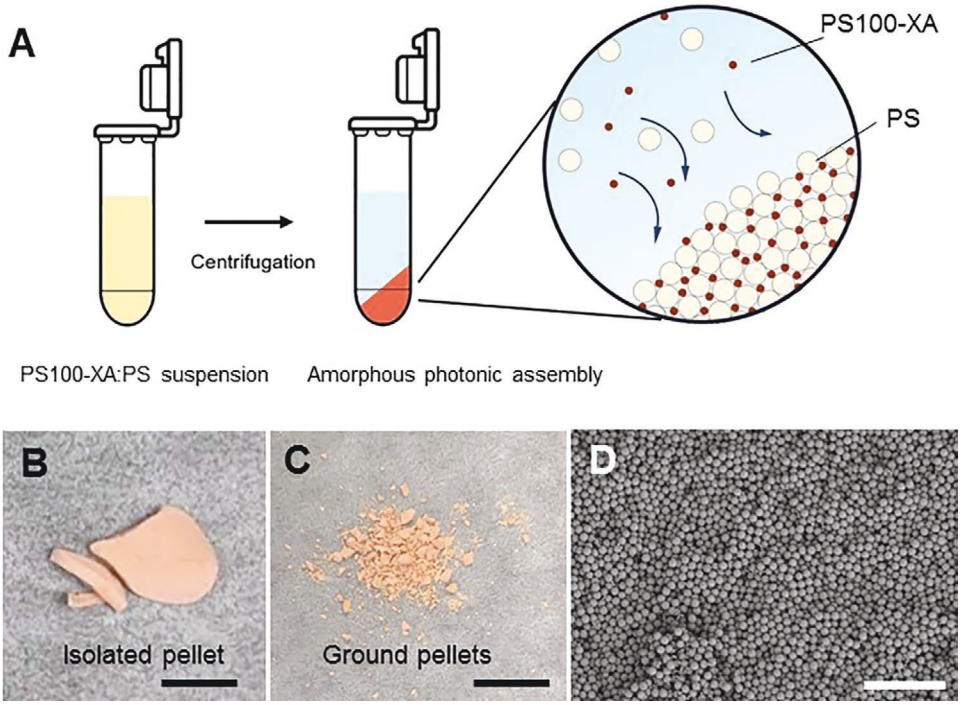

Figure 2. Assembly of the amorphous photonic materials: A) Illustrating the preparation via centrifuging PS100-XA:PS mixtures; photographic images of B) 5% PS100-XA:PS290 pellets (scale bar = 2 mm) and C) powder (scale bar = 2 mm); D) representative SEM micrograph of 5% PS100-XA/PS290 photonic assemblies (scale bar = 250 μm).

color contrast was controlled by the concentration of the PS100-XA nanoparticles (International Commission on Illumination L*a*b (CIELAB) coordinates summarized in Table S2 in the Supporting Information). In each case, the a* (representing red to green chroma), b* (representing yellow to blue chroma), and C* (e.g., purity of color) values of the films increased, as the concentration the PS100-XA nanoparticles increased, suggesting the PS100-XA particle was contributing to the overall "colorfulness" of the films. Without the pigment, the blended PS100 and PS particles presented colors that were similar to the pure, monodispersed PS particles, further supporting that color contrast was controlled by the presence of Xa (Figure S3, Supporting Information). With the pigment, the chromaticity diagram (Figure 3B) also showed that color shifted towards the red/yellow region as the PS100-XA concentration increased. These values differed from the films prepared using pure PS190, PS220, PS260, PS290 nanoparticles, which showed blue, green, yellow, and red color hues, respectively, which agreed with the theoretical wavelengths calculated using Bragg's equation[21] (451, 527, 612, 698 nm for PS190, PS220, PS260, PS290, respectively, Table S3, Supporting Information).

The Xa-based photonic assemblies were further characterized using integrated reflectance spectroscopy (Figure 3C). The addition of PS100-XA nanoparticles lowered the overall integrated reflectance and triggered a red-shifted reflectance peak of 125, 95, 40, and 10 nm with the P190, PS220, PS260, PS290 nanoparticles, respectively. The decrease in the overall integrated reflectance was due to the broad range of light absorption of the PS100-XA particles in the visible light range, as suggested in Figure 1C. This reflectance feature of the PS100-XA materials is likely the main contributor to the perceived red-shift of the blended samples. These trends also agreed with the color space analysis, suggesting that the addition of PS100-XA improved the color contrast of the materials, as it transitioned towards the red/yellow color space. It is also worth noting that the pellets prepared using pure PS particles showed iridescent colors (Figure S4, Supporting Information); however, iridescence disappeared as the PS100-XA content increased above 5 wt% in the PS100-XA:PS mixture. This observation suggested that the absorptive properties of the PS100-XA particles were dominant at concentrations at or above 5 wt% and that these features also contributed to a reduction in the angle-dependent color changes that persist in the monodispersed PS particles alone.

To further investigate this change in angular dependence, we measured the integrated reflectance of drop-casted thin films containing varying ratios of the blended nanoparticles at different angles (**Figure 4**). The drop-casted films produced colors that were consistent with the films prepared using the powdered and pressed pellets. As we originally predicted, the presence of PS100-XA improved the angular independence, where the PS100-XA:PS190, PS100-XA:PS220, PS100-XA:PS260, and PS100-XA:PS290 films exhibited reflectance peaks at 425, 475, 550, and 615 nm regardless of the incident light angles. Conversely, the visible colors reflected from the pure PS nanoparticle films showed a prominent dependency on viewing angle with noticeable 40–60 nm blue-shifted peaks for each condition, as the incident angles increased from 15° to 60° (Figure S5, Supporting Information). Overall, our results supported that the addition of PS100-XA disrupted the

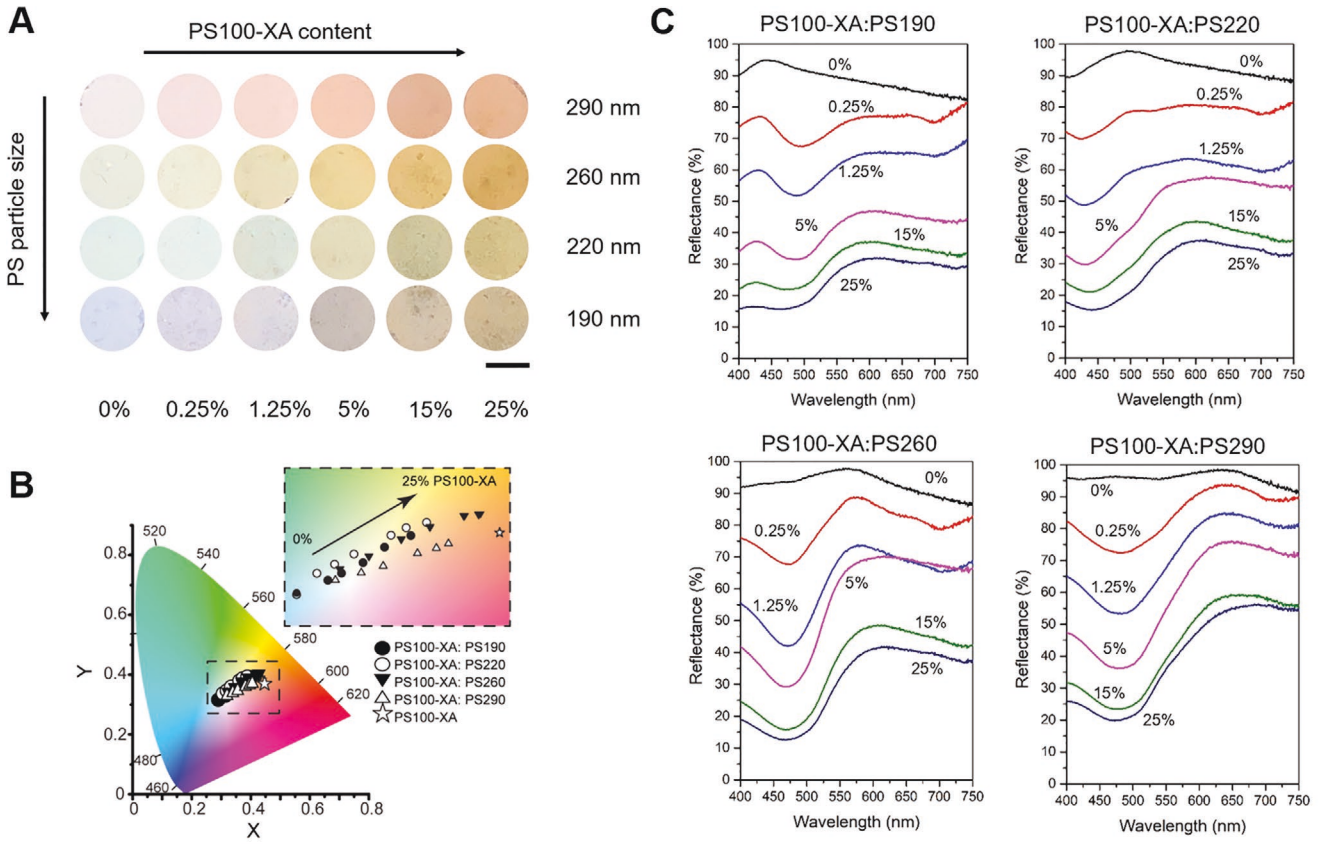

Figure 3. Characterization of the amorphous photonic assemblies containing XA. A) Photographic images of the achievable color palette formed by varying the size of PS nanoparticles (longitudinal direction), and by varying the amount of PS100-XA (horizontal direction) (scale bar = 6 mm). B) CIE 1931 chromaticity diagram of each film, illustrating the color deviation as a function of PS particle size and PS100-XA content. C) Reflectance spectra of the PS100-XA:PS films with varying concentrations PS100-XA and particle size of PS nanoparticles.

natural long-range order of the pure PS nanoparticles, enabling the angle-independent reflectance to propagate from the amorphous photonic assemblies. Specifically, the addition of smaller-sized particles into monodispersed colloidal particles appears to disrupt the long-range order and periodicity and make amorphous particle arrays with short-range order and improved angle independence.[22]

To test the how the surrounding environment and production method impacted the assembly and subsequent photonic properties of the Xa-based materials, the PS100-XA:PS particles

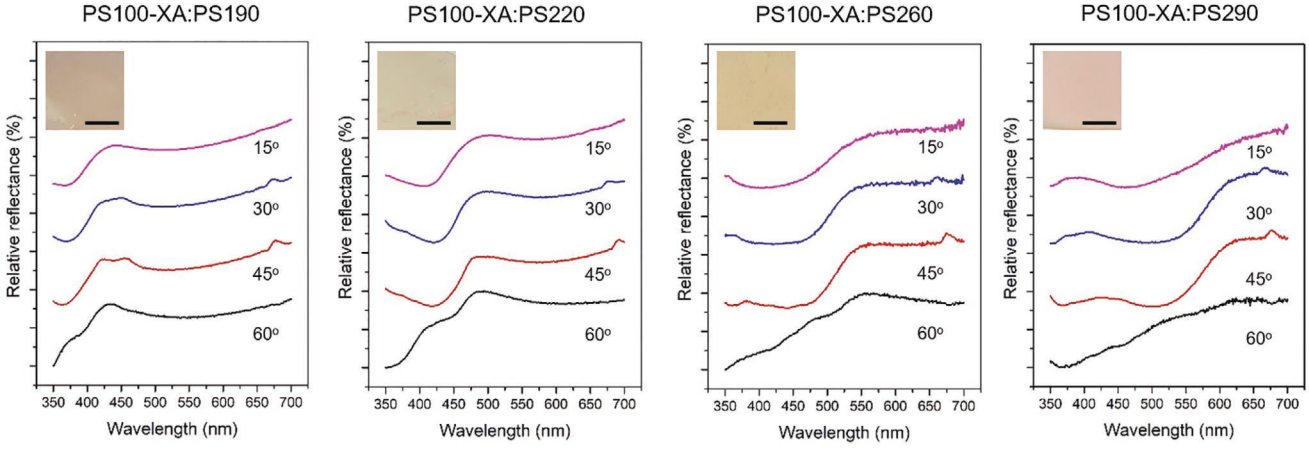

Figure 4. Analysis of incident light on color. Here, reflectance spectra and photographic images (insert, scale bar = 2 mm) of the photonic materials comprising PS100-XA:PS190, PS100-XA:PS220, PS100-XA:PS260, and PS100-XA:PS290 are presented at different light incident angles (PS100-XA: PS ratio = 5% by weight).

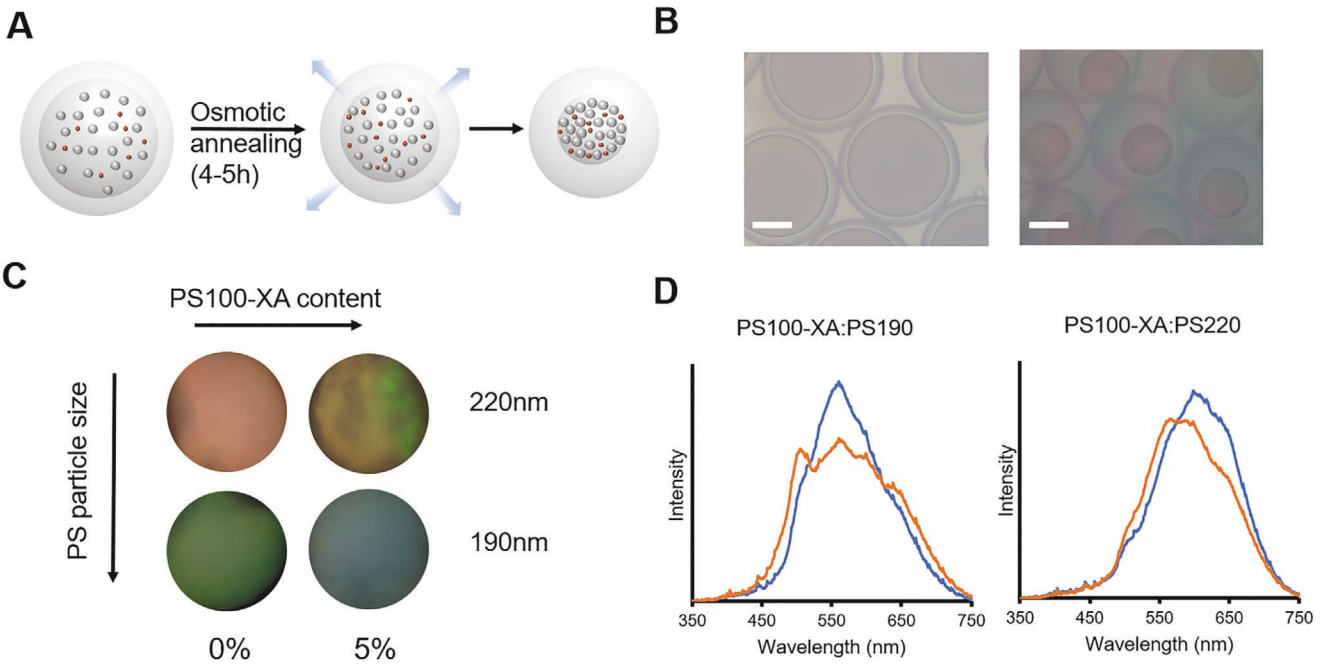

Figure 5. Photonic assemblies in W/O/W double emulsion systems. A) A schematic illustration of photonic assembly formation during osmotic annealing. B) Photographic images of double emulsion droplets before (left) and after (right) osmotic annealing (scale bar = 50 µm). C) Photographic image of the annealed photonic assemblies in double emulsions. D) Reflectance measurement of the photonic assemblies (blue: PS100-XA:PS ratio = 0 wt%, orange: PS100-XA:PS ratio = 5 wt%).

were assembled and manipulated in W/O/W double emulsion droplets using osmotic annealing, with pure monodispersed polystyrene nanoparticles as controls (**Figure 5**). This method has been previously used to produce photonic crystals or glasses from a suspension of uniform colloids, leading to production of photonic balls exhibiting a wide range of colors.[23,24] Double emulsion droplets containing PS100-XA:PS particle mixtures in the inner aqueous phase were fabricated in a glass capillary-based microfluidic device, collected in 1 M NaCl, then slowly annealed over 4–5 h to enable the formation of amorphous photonic assemblies (Figure 5A,B).[23] In this configuration, the outflux of the aqueous phase during osmotic annealing reduced the volume of the inner phase of the droplet and allowed the charged heterogenous particles to assemble. The resultant products prepared using both pure PS nanoparticles and PS100-XA:PS particle mixtures (5 wt% PS100-XA:PS) reflected different colors, where the addition of PS100-XA changed the color of the pure PS photonic assemblies from green to blue and pink to yellow/green for the PS190 and PS220 particles, respectively (Figure 5C). Interestingly, the control PS190 and PS220 photonic assemblies displayed colors that differed from the controls prepared by the centrifugation methods in air. These particles did not crystalize in confined droplets but instead formed amorphous photonic structures with angle-independent reflectance peaks at 550 and 610 nm for the PS190 and PS220 nanoparticles, respectively (Figure 5D; Figure S6, Supporting Information). This red-shift of the reflected light was likely caused by the larger interparticle distances and the presence of water between particles—both of which would increase the effective refractive index of the medium as predicted by the single scattering model of Magkiriadou et al.,[20,25] where $n_{\text{eff/water}} = 1.49$ and $n_{\text{eff/air}} = 1.42$. These trends reversed when the PS100-XA nanoparticles were incorporated at a 5 wt% density. We observed that the PS190 and PS220 photonic assemblies contributed to a blue-shift in color space, rather than the red-shift observed using the centrifugation methods (Figure 5C,D). This phenomenon is likely also caused by the change in packing configurations from the bidispersed system due to a reduction in the volume fraction of the larger PS particles when the smaller PS100-XA particles were added.[26] Similar trends have also been observed when doping small-sized nanoparticles in bidispersed SiO_2 nanoparticle colloidal photonic crystals.[22]

Despite these differences, the results showed that the coloration effects from configuration changes were again dominated by the pigmentary contribution of the PS100-XA. Curiously, "Janus" dual colors of yellow and green were observed in the PS100-XA:PS220 samples, suggesting a dual packaging configuration of the amorphous photonic assemblies was present within the same double emulsion droplet. The dual colors were also likely caused by different orientations of crystalline assembly. It has been observed that such phase separations tend to occur in binary colloidal systems both with or without the presence of polymer during a slow annealing process.[27] We speculate that a similar phase separation has occurred within the PS100-XA:PS220 particle mixtures during our annealing and that such a process leads to formation of a PS-rich fraction and a PS-poor fraction, yielding "Janus" assemblies within the emulsion droplets. While more work, including the application of high-resolution imaging to resolve specific interparticle distances within the double emulsions, is needed to fully understand these interesting findings, for now we can agree that the

presence of PS100-XA nanoparticles is able to impact the coloration of colloidal photonic assemblies in both powdered and aqueous medium, introducing a new method to generate angle-independent structural colors in multiple environments.

3. Conclusion

Several attempts to improve the color contrast of synthetic photonic crystals have succeeded using small, black particles such as carbon black,[18] ferric oxide,[28] pyrrole polymers,[29] and melanin-based nanomaterials[6–10] to suppress incoherent light scattering and enhance high-visibility structural colors. Unlike these broad-band absorbers, nonblack pigments like xanthommatin and even pterins offer spectral selectivity and performance as high-pass optical filters to further diversify the range of addressable colors in synthetic photonic materials. Specifically, in our study we observed that color, color contrast, and angular independence were controlled by the addition of the Xa tethered to PS100 nanoparticles, illustrating an important role of Xa based pigments in modulating coloration in artificial photonic assemblies. While our findings on their own introduce a new application space for this class of compounds, we also draw important insights into why these molecules are often found packaged as heterogenous distributions of nanoparticles in natural systems. That is that the pigment/particle combination contributes to diversification of visible colors originating from the same biomolecule. Future experiments will expand on these preliminary findings, as we also explore optical simulations to better understand the performance properties of such Xa-based photonic materials.

4. Experimental Section

Materials: Carboxylic acid functionalized PS nanoparticles (100 nm) were purchased from PolyScience (Niles, IL). Potassium ferrocyanide, potassium phosphate dibasic, potassium phosphate monobasic, hydrochloric acid, sodium hydroxide, styrene, sodium styrene sulfonate (NaSS), DMSO-d_6, 2-(N-morpholino)ethanesulfonic acid (MES), and potassium persulfate were purchased from Fisher Scientific (Hampton, NH). Trifluoroacetic acid, 3-hydroxykynureinine, 1-Ethyl-3-(3-dimethylaminopropyl) carbodiimide (EDC) were purchased from Sigma-Aldrich (St. Louise, MO).

Synthesis of Xa Pigment: Xa was synthesized via the cyclization of 3-hydroxykynurenine according to previous procedures but with modifications.[15,30] Briefly, a 17.8×10^{-3} M 3-hydroxykynurenine solution was prepared in 0.1 M potassium phosphate buffer (pH 7.0). Next, potassium ferrocyanide (78.1×10^{-3} M) was added dropwise into the 3-hydroxykynurenine solution then stirred at room temperature for 2.5 h. The product was precipitated using 1 N hydrochloric acid, washed 3 times in 0.2 N hydrochloric acid, dried in a fume hood overnight, and stored at 4 °C until further use. Proton NMR spectrum of the pigment was collected in DMSO-d_6 containing 4% trifluoroacetic acid using a 500 MHz Nuclear Magnetic Resonance (NMR) spectrometer (Varian, Palo Alto, Ca) (Figure S7, Supporting Information). The product, Xa, displayed characteristic peaks at 8.4, 8.0, 7.8, 7.7, 6.7, 4.6, 3.9 ppm, which were in agreement with our previous reports.[15,31] The molecular weight of the product was analyzed using a liquid chromatography-mass spectrometry (LC-MS) (Thermo LTQ Orbitrap XL, Thermo Fisher Scientific, Waltham, MA) (Figure S8, Supporting Information). The m/z value of the major peak in the chromatograph was determined to be 424.078, in agreement with the molecular weight of Xa.

Synthesis of Xa Functionalized Nanoparticles: Xa functionalized nanoparticles were synthesized via EDC coupling of Xa onto carboxylic acid functionalized PS nanoparticles (Figure 1A). Briefly, EDC (5 mg mL^{-1}) was added into a 2.5 wt% 100 nm carboxylic acid-functionalized polystyrene (PS100) in 0.05% SDS suspension, and the mixture was stirred at room temperature for 30 min. Then, Xa (2 mg mL^{-1}) in 0.1 M MES buffer (pH 5.5) was added into the mixture and stirred for another 2.5 h to tether the Xa pigment onto PS100. After the reaction was completed, the Xa functionalized polystyrene particles (PS100-XA) were cleaned by dialyzing against DI water. The dialyzed PS100-XA particle suspension was further centrifuged at 3000 g for 15 min, washed with DI water three times, then stored in 5 mL of 0.05% SDS. Particle sizes were analyzed using a scanning electron microscopy (SEM) (Hitachi S4800, Tokyo, Japan). The surface charge of the particles during the reaction was analyzed using zeta-potential analysis in a Malvern Nano-ZS90 zetasizer (Malvern, United Kingdoms). The surface chemistry of the particles before and after Xa functionalization was analyzed using Attenuated Total Reflectance-Fourier-transform infrared spectroscopy (ATR-FITR) spectrometry (Bruker Alpha, Bruker Corporation, Billerica, MA) at a resolution of 4 cm^{-1} (32 scans) backgrounded against air.

Synthesis of Polystyrene Nanoparticles: Monodispersed PS nanoparticles of four different sizes were synthesized by surfactant-free emulsion polymerization according to previous protocols,[32] with a detailed reaction recipe provided in Table S4 in the Supporting Information. Briefly, 11.73 g of styrene monomer was added into 200 mL of DI water in a 500 mL round bottom flask. Sodium styrene sulfonate (NaSS,10.3-30.6 mg) was added, and the mixture was degassed using nitrogen gas for 30 min. After degassing, 270 mg of potassium persulfate dissolved in 2 mL of DI water was injected into the mixture through a syringe to initiate the reaction at 80 °C with constant stirring for 24 h to complete the reaction. The particle size, polydispersity index (pdi), and zeta potential of the nanoparticles were determined using a Malvern Nano-ZS90 zetasizer. Particle sizes were further verified using SEM (Figure S9, Supporting Information). Four different sizes of monodispersed PS nanoparticles were synthesized with particle diameter determined to be 189.1 ± 1.7 nm (PS190), 221.2 ± 2.8 nm (PS22), 256.9 ± 5.1 nm (PS260), and 292.6 ± 6.1 nm (PS290).

Preparation of the Amorphous Photonic Assemblies: The Xa-based materials was prepared by centrifuging mixtures of PS100-XA nanoparticles and monodispersed polystyrene nanoparticle suspensions (illustration in Figure S10 in the Supporting Information). PS100-XA nanoparticles and PS nanoparticles were mixed at ratios that ranged from 0% to 25% by weight in 0.05% SDS. The mixtures were sonicated for 1 h followed by centrifugation at 10 000 g for 15 min. The supernatant was aspirated, and the pellets were dried in an 80 °C oven for 16 h to assemble the photonic materials. The resultant product was then recovered, ground into powder and sandwiched between two microscopic slides to press them into round films of 8 mm in diameter. For reflectivity measurements at multiple angles, films containing the variable PS sizes at a constant PS100-XA: PS ratio (5 wt%) were drop-casted as photonic films.

The Xa-based assemblies in droplets were fabricated using a glass capillary based microfluidic device to prepare water-in-oil-in-water (W/O/W) double emulsions, following a previously described method.[23] In this case, the diameters of the injection and the collection capillaries were adjusted to be 120 and 200 μm, respectively. To generate the W/O/W double emulsions, three different fluids were introduced into the microfluidic device by syringe pumps. The inner fluid was an aqueous suspension of polystyrene nanoparticle mixtures (PS100-XA: PS ratio = 5 wt%) in 0.05 wt% SDS. The concentration of PS suspension was adjusted to be around 5 wt%. The middle fluid contained 75 wt% two-part silicone rubber, 23 wt% PDMS oil and 2 wt% Dow Corning 749 surfactant. The outer fluid was a 2 wt% PVA and 10 wt% glycerol aqueous solution. The flow rates in the inner, middle, and outer fluids were set at 2, 2, and 40 mL h^{-1}, respectively. The generated double emulsions were collected in 1 M NaCl solutions to induce osmotic annealing.[23,24] Optical microscopic images of the spherical photonic structures and their reflectance spectra were obtained by using an upright microscope (Carl Zeiss Axio Plan II) equipped with a CCD camera, and a fiber-coupled spectrometer (Laboratory Spectrometer, Edmund Optics).

Optical Characterization: The International Commission on Illumination L*a*b (CIELAB) coordinates[33] of the photonic films was measured using an Ocean Optics UV-Vis-shortwave NIR spectrophotometer (200–800 nm), equipped with a 45° diffuse reflectance probe, a certified diffuse reflectance standard (Labsphere), and a standard illuminant A. The CIELAB coordinate values were collected against a white standard reference (WS-1). All reflectance spectra were collected using an Evolution 220 spectrophotometer (Thermo Scientific, Waltham, MA) equipped with an ISA-220 integrated sphere accessory. Multiangle reflectivity measurements were conducted using 15°, 30°, 45°, and 60° fixed angle accessories, wherein each sample was manually placed on the calibrated accessory prior to data acquisition. In this configuration, incident beams were cast onto the surface of the photonic films at each angle, and the specular reflectance of the corresponding angles were collected. All reflectance spectra were collected at a bandwidth of 2 nm with a spectral resolution of 1 nm.

Supporting Information

Supporting Information is available from the Wiley Online Library or from the author.

Acknowledgements

This work was supported in part by the Army Research Office (Award W911NF-16-1-0455) and the National Science Foundation (Award DMR-1712345).

Conflict of Interest

The authors declare no conflict of interest.

Data Availability Statement

The data that support the findings of this study are available from the corresponding author upon reasonable request.

Keywords

bio-inspired, cephalopods, photonic assemblies, pigments, structural colors

Received: February 28, 2021
Revised: August 25, 2021
Published online: September 24, 2021

[1] a) S. Kinoshita, S. Yoshioka, *ChemPhysChem* **2005**, *6*, 1442; b) M. D. Shawkey, N. I. Morehouse, P. Vukusic, *J. R. Soc. Interface* **2009**, *6*, S221.
[2] a) D. G. Stavenga, H. L. Leertouwer, N. J. Marshall, D. Osorio, *Proc. R. Soc. London Ser. B* **2011**, *278*, 2098; b) M. Xiao, A. Dhinojwala, M. Shawkey, *Opt. Express* **2014**, *22*, 14625.
[3] B. D. Wilts, B. Wijnen, H. L. Leertouwer, U. Steiner, D. G. Stavenga, *Adv. Opt. Mater.* **2017**, *5*, 1600879.
[4] N. I. Morehouse, P. Vukusic, R. Rutowski, *Proc. Biol. Sci.* **2007**, *274*, 359.
[5] T. L. Williams, S. L. Senft, J. Yeo, F. J. Martin-Martinez, A. M. Kuzirian, C. A. Martin, C. W. DiBona, C. T. Chen, S. R. Dinneen, H. T. Nguyen, C. M. Gomes, J. J. C. Rosenthal, M. D. MacManes, F. Chu, M. J. Buehler, R. T. Hanlon, L. F. Deravi, *Nat. Commun.* **2019**, *10*, 1004.
[6] Y. Zhang, B. Dong, A. Chen, X. Liu, L. Shi, J. Zi, *Adv. Mater.* **2015**, *27*, 4719.
[7] M. Xiao, Y. Li, M. C. Allen, D. D. Deheyn, X. Yue, J. Zhao, N. C. Gianneschi, M. D. Shawkey, A. Dhinojwala, *ACS Nano* **2015**, *9*, 5454.
[8] M. Xiao, Z. Hu, Z. Wang, Y. Li, A. D. Tormo, N. L.e Thomas, B. Wang, N. C. Gianneschi, M. D. Shawkey, A. Dhinojwala, *Sci. Adv.* **2017**, *3*, e1701151.
[9] P. Liu, J. Chen, Z. Zhang, Z. Xie, X. Du, Z. Gu, *Nanoscale* **2018**, *10*, 3673.
[10] A. Kawamura, M. Kohri, G. Morimoto, Y. Nannichi, T. Taniguchi, K. Kishikawa, *Sci. Rep.* **2016**, *6*, 33984.
[11] T. L. Williams, C. W. DiBona, S. R. Dinneen, S. F. Jones Labadie, F. Chu, L. F. Deravi, *Langmuir* **2016**, *32*, 3754.
[12] a) R. Futahashi, R. Kurita, H. Mano, T. Fukatsu, *Proc. Natl. Acad. Sci. USA* **2012**, *109*, 12626; b) M. Osanai-Futahashi, K. i. Tatematsu, R. Futahashi, J. Narukawa, Y. Takasu, T. Kayukawa, T. Shinoda, T. Ishige, S. Yajima, T. Tamura, K. Yamamoto, H. Sezutsu, *Heredity* **2016**, *116*, 135; c) M. Riou, J.-P. Christidès, *J. Chem. Ecol.* **2010**, *36*, 412.
[13] S. R. Dinneen, R. M. Osgood, M. E. Greenslade, L. F. Deravi, *J. Phys. Chem. Lett.* **2017**, *8*, 313.
[14] S. P. Aubourg, W. Torres-Arreola, M. Trigo, J. M. Ezquerra-Brauer, *Eur. J. Lipid Sci. Technol.* **2016**, *118*, 1293.
[15] A. Kumar, T. L. Williams, C. A. Martin, A. M. Figueroa-Navedo, L. F. Deravi, *ACS Appl. Mater. Interfaces* **2018**, *10*, 43177.
[16] S. Zhu, U. Panne, K. Rurack, *Analyst* **2013**, *138*, 2924.
[17] C. A. Martin, Z. Lin, A. Kumar, S. R. Dinneen, R. M. Osgood, L. F. Deravi, *ACS Appl. Bio Mater.* **2021**, *4*, 507.
[18] Y. Takeoka, S. Yoshioka, A. Takano, S. Arai, K. Nueangnoraj, H. Nishihara, M. Teshima, Y. Ohtsuka, T. Seki, *Angew. Chem., Int. Ed. Engl.* **2013**, *52*, 7261.
[19] G. H. Lee, J. B. Kim, T. M. Choi, J. M. Lee, S. H. Kim, *Small* **2019**, *15*, 1804548.
[20] S. H. Kim, S. Magkiriadou, D. K. Rhee, D. S. Lee, P. J. Yoo, V. N. Manoharan, G. R. Yi, *ACS Appl. Mater. Interfaces* **2017**, *9*, 24155.
[21] P. A. Rundquist, P. Photinos, S. Jagannathan, S. A. Asher, *J. Chem. Phys.* **1989**, *91*, 4932.
[22] M. Harun-Ur-Rashid, A. Bin Imran, T. Seki, M. Ishii, H. Nakamura, Y. Takeoka, *ChemPhysChem* **2010**, *11*, 579.
[23] S. J. Yeo, F. Tu, S. H. Kim, G. R. Yi, P. J. Yoo, D. Lee, *Soft Matter* **2015**, *11*, 1582.
[24] a) T. M. Choi, J.-G. Park, Y.-S. Kim, V. N. Manoharan, S.-H. Kim, *Chem. Mater.* **2015**, *27*, 1014; b) S. H. Kim, J. G. Park, T. M. Choi, V. N. Manoharan, D. A. Weitz, *Nat. Commun.* **2014**, *5*, 3068.
[25] S. Magkiriadou, J.-G. Park, Y.-S. Kim, V. N. Manoharan, *Opt. Mater. Express* **2012**, *2*, 1343.
[26] R. S. Farr, R. D. Groot, *J. Chem. Phys.* **2009**, *131*, 244104.
[27] a) I. Zhang, R. Pinchaipat, N. B. Wilding, M. A. Faers, P. Bartlett, R. Evans, C. P. Royall, *J. Chem. Phys.* **2018**, *148*, 184902; b) H. Wang, Y. Liu, Z. Chen, L. Sun, Y. Zhao, *Sci. Adv.* **2020**, *6*, eaay1438.
[28] D. Yang, W. Luo, Y. Huang, S. Huang, *ACS Omega* **2019**, *4*, 528.
[29] X. Yang, D. Ge, G. Wu, Z. Liao, S. Yang, *ACS Appl. Mater. Interfaces* **2016**, *8*, 16289.
[30] F. Figon, T. Munsch, C. Croix, M.-C. Viaud-Massuard, A. Lanoue, J. Casas, *Insect Biochem. Mol. Biol.* **2020**, *124*, 103403.
[31] T. L. Williams, S. A. Lopez, L. F. Deravi, *ACS Sustainable Chem. Eng.* **2019**, *7*, 8979.
[32] a) R. K. Shah, H. C. Shum, A. C. Rowat, D. Lee, J. J. Agresti, A. S. Utada, L.-Y. Chu, J.-W. Kim, A. Fernandez-Nieves, C. J. Martinez, *Mater. Today* **2008**, *11*, 18; b) J. Fang, Y. Xuan, Q. Li, *Sci. China: Technol. Sci.* **2010**, *53*, 3088.
[33] a) M. R. Luo, in *Encyclopedia of Color Science and Technology* (Ed: R. Luo), Springer Berlin Heidelberg, Berlin, Heidelberg **2014**, p. 1; b) M. McLellan, L. Lind, R. Kime, *J. Food Qual.* **1995**, *18*, 235.